Earthquakes and Structures, *Vol. 17, No. 4 (2019) 411-424*
DOI: https://doi.org/10.12989/eas.2019.17.4.411

Dynamic response and waterproof property of tunnel segmental lining subjected to earthquake action

Qixiang Yan[1a], Rui Bao[2], Hang Chen[*3], Binjia Li[1], Wenyu Chen[1], Yongwen Dai[4] and Hongyuan Zhou[4]

[1]Key Laboratory of Transportation Tunnel Engineering, Southwest Jiaotong University, Ministry of Education, Chengdu 610031, China
[2]Beijing Urban Construction Design & Development Group Co., Ltd., Beijing 100037, China
[3]Sichuan Highway Planning, Survey, Design and Research Institute Co., Ltd., Chengdu 610041, China
[4]China Water Conservancy and Hydropower Seventh Engineering Bureau Co., Ltd., Chengdu 610213, China

(*Received November 12, 2018, Revised February 2, 2019, Accepted September 4, 2019*)

Abstract. In this study, a numerical model of a shield tunnel with an assembled segmental lining was built. The seismic response of the segmental lining of the section of the shield tunnel in Line 1 of the Chengdu Metro is analyzed as it passes through the interface of sand-cobble and mudstone layers. To do so, the node-stress seismic-motion input method was used to input the seismic motion measured during the 2008 Wenchuan earthquake, and the joint openings and dislocations associated with the earthquake action were obtained. With reference to the Ethylene-Propylene-Diene Monomer (EPDM) sealing gaskets used in the shield tunnels in the Chengdu Metro, numerical simulation was applied to analyze the contact pressure along the seepage paths and the waterproof property under different joint openings and dislocations. A laboratory test on the elastic sealing gasket was also conducted to study its waterproof property. The test results accord well with the numerical results and the occurrence of water seepage in the section of the shield tunnel in Line 1 of the Chengdu Metro during the 2008 Wenchuan earthquake was verified. These research results demonstrate the deformation of segmental joint under earthquake, also demonstrate the relationship between segmental joint deformation and waterproof property.

Keywords: segmental lining; node-stress seismic-motion input method; joint deformation; elastic sealing gasket; waterproof property

1. Introduction

In theory, tunnel structures have better seismic performance than above ground structures (Koizumi 2009). However, the many strong earthquakes over the globe in the past 30 years have caused damage to the tunnels in earthquake-affected areas, including the Kobe earthquake in Japan (Hashash *et al*. 2001), Duzce earthquake in Turkey (Kontoe *et al*. 2008), Chi-Chi earthquake in Taiwan (Wang *et al*. 2001), Wenchuan earthquake in China (Li 2012, Lai *et al*. 2017), and Kumamoto earthquake in Japan (Zhang *et al*. 2018). The 2008 Wenchuan earthquake, in particular, not only destroyed many mountain tunnels near the epicenter but also caused leakages at some segmental joints and segmental bolt holes of the shield tunnel in the Chengdu Metro. Therefore, to ensure the structural integrity and waterproof design of shield tunnels affected by high-intensity earthquakes, it is important to study the dynamic characteristics of shield tunnels, their segmental joint deformation, and their waterproof property after joint deformation.

Many researchers have studied the dynamic response of tunnel structures subjected to earthquake action. The authors of papers (Balendra *et al*. 1984, Pakbaz and Yareevand 2005, Amorosi and Boldini 2009, Fattah *et al*. 2015, Gomes *et al*. 2015) focused on two-dimensional analyses of the transverse dynamic behavior of tunnel structures. To analyze longitudinal deformation, some researchers (Yu *et al*. 2016, Shen *et al*. 2016, Yang *et al*. 2013, Tao *et al*. 2015) built three-dimensional (3D) finite-element models to determine the seismic response of mountain tunnels. Ding *et al*. (2006) analyzed the flexible joint deformation of an immersed tunnel under seismic loading. The researchers (Luco and Barros 1994, Stamos and Beskos 1996) numerically analyzed the dynamic response of a 3D circular tunnel. Li and Song (2015) used numerical modelling techniques to analyze the longitudinal response of tunnels under an asynchronous seismic wave. Fabozzi and Bilotta (2016) studied the performance of continuous and segmental linings of shallow tunnels under seismic loading. Hatzigeorgiou and Beskos (2010) investigated the seismic soil-structure interaction in 3D lined tunnels. The authors used numerical simulation to analyze the dynamic response of a 3D circular tunnel lining and the soil-structure interaction subjected to earthquake action. However, their research was based on the homogenous ring model of the tunnel structure and the shield tunnel lining as a prefabricated assembled structure, without taking into consideration the connection joints. In the papers (Guo *et al*. 2006, Yu *et al*. 2013a, b, 2017), the authors considered the effect of the segmental joints of

*Corresponding author, M.S.
E-mail: chenhangssd@163.com
[a]Ph.D.
E-mail: 764365015@qq.com

Copyright © 2019 Techno-Press, Ltd.

ISSN: 2092-7614 (Print), 2092-7622 (Online)

shield tunnels. However, Guo *et al*. (2006) only analyzed the stress distribution of the shield tunnel lining subjected to earthquake action without analyzing the segmental joint deformation. Yu *et al*. (2013a, b, 2017) investigated the influence of non-uniform seismic excitation and flexible joints on the dynamic response of the shield tunnel structure and analyzed the stress experienced by the segmental lining and the deformation of the circumferential joints. However, these authors did not analyze the deformation of the longitudinal joints or the distribution of the openings and dislocations at different positions on the circumferential joints.

Regarding the elastic sealing gaskets used in shield tunnels, many researchers have investigated their mechanical properties and waterproof property. Shalabi *et al*. (2012, 2016) investigated the gasket-in-groove mechanical and sealant behaviors in water leakage tests and developed a conceptual model that explained the leakage behavior of the gasket-in-groove. However, these authors' research paid more attention to the waterproof property of the sealing gaskets in the single designed condition, considering only joint opening and neglecting the effect of joint dislocation. Ding *et al*. (2017) studied the waterproof property of the segmental joint with respect to simultaneous joint opening and dislocation and analyzed the influence of the sealing gasket's inner structure on waterproof property. Wang (2015) used numerical simulation to analyze the waterproof failure mechanism of the rubber sealing gasket, but only for singe cases of joint opening or dislocation. Existing research on elastic sealing gaskets has mostly focused on their waterproof property without studying the distribution of the contact pressure between sealing gaskets and between the sealing gasket and segmental sealing groove. Nor have the relationship between the joint opening and dislocation of shield tunnels subjected to earthquake action and the waterproof property of the elastic sealing gasket been further studied.

The main objectives of this study are as follows: (1) Based on a section of Line 1 of the Chengdu Metro shield tunnel passing through the interface between sand-cobble and mudstone layers, a partial refined model of an assembled segmental lining is built, using the spring and contact surface to simulate the joint bolt and segmental joint surface, respectively. The structural analysis model of the shield tunnel is developed by combining a partially refined model of the assembled segmental lining with a model of its structural equivalent flexural rigidity. (2) Considering the

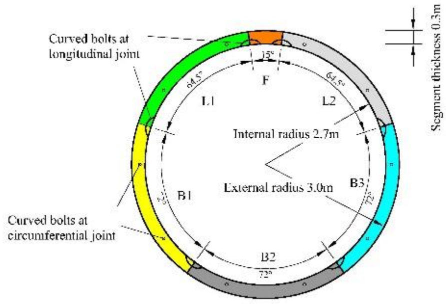

Fig. 1 Cross-section of the shield tunnel lining

influence of the near-field-measured three-directional seismic motion near the Chengdu Metro, the segmental joint deformation is investigated, using the node-stress input method, to study the dynamic response of the segmental lining to earthquake action. (3) Based on the Mooney-Rivlin constitutive model, a numerical model is developed to analyze the waterproof property of the elastic sealing gasket under different joint openings and dislocations. (4) A laboratory test on the elastic sealing gasket to determine its waterproof property under different joint openings and dislocations is conducted; and the water seepage that had occurred in some segmental joints of the shield tunnel in Line 1 of the Chengdu Metro during the 2008 Wenchuan earthquake is verified.

2. Project background

The city of Chengdu, capital of Sichuan province, is located in the southwest of China. Construction began on Line 1 of the Chengdu Metro in 2005 and a large number of shield tunnels had been completed by 2008 when the Wenchuan earthquake occurred. The Metro Line 1 is a north-south metro line in Chengdu. Most of its shield tunnels go through a sand-cobble layer but some sections pass through the interface between sand-cobble and mudstone layers. The sand-cobble layer, which is filled with sand, has good water permeability and fissures in the mudstone layer are well developed. The burial depth of the shield tunnel is 12 m and the water level over the shield tunnel is 10 m.

Fig. 1 shows a typical cross section of a segmental lining structure in Line 1 of the Chengdu Metro. The

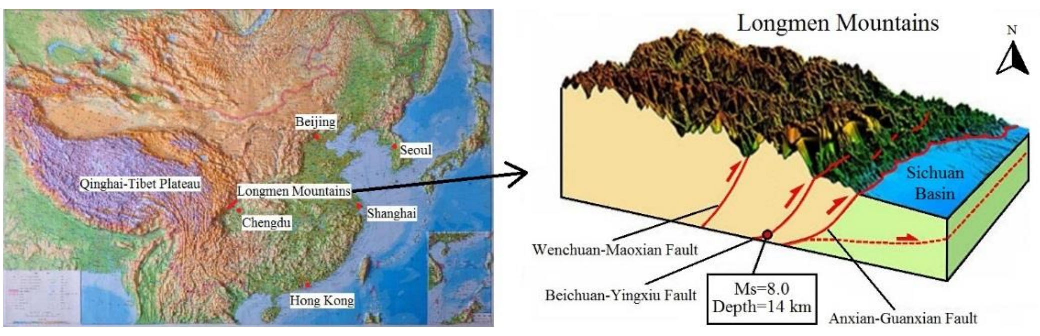

Fig. 2 Seismogenic faults of Wenchuan earthquake

Table 1 Material parameters

Material type	Elastic modulus/MPa	Poisson's ratio	Density/kg/m^3	Angle of friction/∘	Cohesion/kPa	S-wave velocity/m/s	P-wave velocity/m/s
Sand-cobble	25	0.35	2200	35	5	64.9	135
Mudstone	2000	0.25	2300	38	700	590	1020
Lining concrete	34500	0.2	2500	-	-	2400	3920

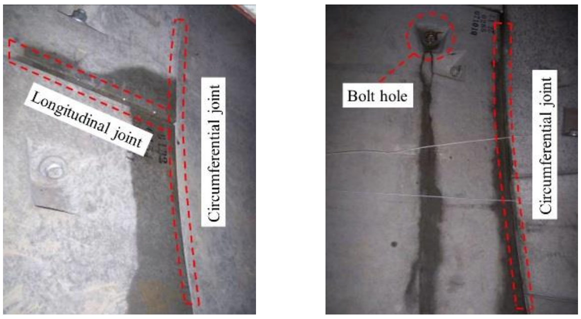

(a) Circumferential joint (b) Bolt hole

Fig. 3 Water seepage in segmental lining after earthquake

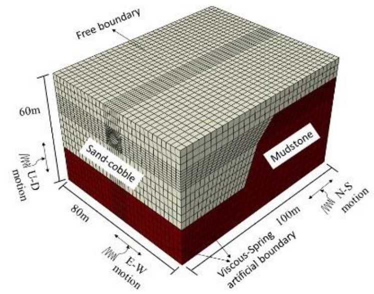

Fig. 4 Numerical analysis model

external and internal diameters of the tunnel are 6 m and 5.4 m, respectively, and the segment thickness and width are 0.3 m and 1.5 m, respectively. A segmental lining ring consists of three standard segments B1-B3, two counter key segments L1-L2, and one key segment F. Each longitudinal joint between adjacent segments is connected by two curved bolts, and each circumferential joint between adjacent segmental lining rings is connected by 10 curved bolts. The diameter of the curved bolts is 24 mm.

In 2008, the Wenchuan earthquake occurred in the Longmen Mountains fault zone in Sichuan. The Richter scale value of the Wenchuan earthquake is 8.0 and the focal depth is approximately 14.0 km. The Longmen Mountains fault zone, comprising the Anxian-Guanxian Fault, Beichuan-Yingxiu Fault, and Wenchuan-Maoxian Fault, is the result of a nappe thrusting to the southeast with a clockwise shearing action. The tectonic stress that had accumulated over the long term in the Beichuan-Yingxiu Fault suddenly released, causing the Wenchuan earthquake, as shown in Fig. 2.

The city of Chengdu is 73.0 km away from the town of Yingxiu, which is the epicenter of the Wenchuan earthquake. The Metro interval tunnel in Chengdu is the shield tunnel closest to the epicenter. The earthquake did not cause severe damage to the main structure of the Metro Line-1 shield tunnel, but water leakage occurred after the Wenchuan earthquake at some segmental joints and segmental bolt holes in the section of the shield tunnel passing through the interface between sand-cobble and mudstone layers, as shown in Fig. 3. The water seepage occurred mainly in the circumferential joints near the arch of the shield tunnel and in a few bolt holes nearby.

3. Numerical model of dynamic analysis

Using as a basis the abovementioned section of the shield tunnel in Line 1 of the Chengdu Metro passing though the interface between the sand-cobble and mudstone layers, a numerical model was built to analyze the dynamic response of the segmental lining and the deformation of the segmental joints. Fig. 4 shows this numerical model for seismically analyzing the shield tunnel. The length, width, and height of the model tunnel were 100 m, 80 m, and 60 m, respectively, and its burial depth was 12 m. Subway Line 1 of the Chengdu Metro runs approximately north-south, so the longitudinal and horizontal cross-sectional directions of the tunnel are north-south and east-west, respectively. Eight-node 3D hexahedral elements with reduced integration (C3D8R) were used to simulate the soil and segmental lining. There were 108,272 elements in the numerical model. The Mohr-Coulomb elastoplastic constitutive model was considered for the surrounding ground, while the elastic constitutive model was adopted for the segmental lining. The physical and mechanical properties of the surrounding ground, lining are summarized in Table 1.

3.1 Artificial boundary of the numerical model

To simulate the continuity of the strata surrounding the tunnel, a viscous-spring artificial boundary around and at the bottom of the model was used, and the top model boundary was left free. The viscous-spring artificial boundary is equivalent to a continuous-distribution parallel spring-damper system. The stiffness and damping coefficient of the normal and tangential springs on the artificial boundary were determined by the following formula (Li and Song 2015)

$$\begin{cases} k_N = \alpha_N \frac{G}{R} \\ c_N = \rho c_p \end{cases} \tag{1}$$

$$\begin{cases} k_T = \alpha_T \frac{G}{R} \\ c_T = \rho c_s \end{cases} \tag{2}$$

where $c_p = \sqrt{\frac{E(1-\mu)}{\rho(1+\mu)(1-2\mu)}}$, $c_s = \sqrt{\frac{G}{\rho}}$. k_N and k_T are the

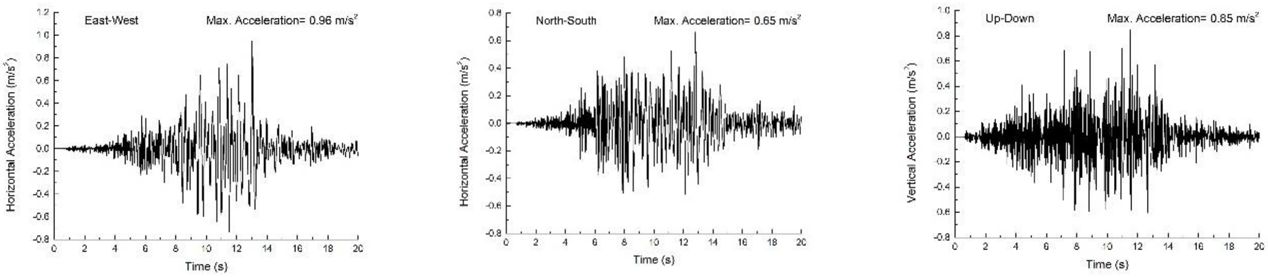

(a) E-W acceleration (b) N-S acceleration (c) U-D acceleration

Fig. 5 Acceleration records at the Zhonghe strong-motion station

normal and tangential spring stiffness, respectively; c_N and c_T are the normal and tangential damping coefficients, respectively; R is the distance from the wave source to the artificial boundary point; c_p and c_s are the velocity of the P-wave and S-wave of the medium, respectively; ρ is the medium mass density; G is the shear modulus; and α_N and α_T are the normal and tangential viscous-spring boundary correction factors, respectively (α_N=1.0-2.0 and α_T= 0.5-1.0; in this study $\alpha_N = 1.33$ and $\alpha_T = 0.67$). E is the elastic modulus and μ is the Poisson's ratio.

3.2 Input method of seismic motion

For the seismic-motion input, the conventional method is to approximately input the acceleration of three vertical directions measured at a nearby seismic station, assuming that the seismic wave arises vertically from the base. Fig. 5 shows a plot of the bedrock accelerations recorded at the Zhonghe strong-motion station in Chengdu, including north-south, east-west, and vertical. The maximum acceleration in the east-west, north-south, and up-down directions were 0.96 m/s^2, 0.65 m/s^2, and 0.85 m/s^2, respectively. The duration of the seismic motion was 20 s.

The above conventional seismic-motion input method was derived based on the seismic characteristics of the ground structure. This method need only apply the corresponding acceleration to the bottom of the model, while neglecting the seismic-motion input of the nodes on the lateral boundaries. The seismic response of underground structures, such as the shield tunnel, is very different from that of the ground structure, so factors such as the seismic motion of the nodes on the lateral boundary and the reflection of seismic waves on the free surface greatly influence the seismic analysis of underground structures. In this paper, the node-stress seismic-motion input method was adopted (Zhao *et al* 2010, Huang *et al*. 2010). Considering the phase difference and reflection of the seismic waves, here, the seismic-motion input method is presented on the basis of the wave-field separation technique and viscoelastic artificial boundary conditions. This method can guarantee that the stress and displacement at the boundary nodes are consistent with the actual values and fit well with the viscous-spring artificial boundary (Zhao *et al* 2010). The above acceleration time history curves were converted to node stress using this method and then the ABAQUS program was used to apply stress to the nodes on the boundary.

Shear waves, which travel vertically upward from the bottom of the model, can be decomposed into two directions: E-W and N-S, which correspond to two-directional acceleration curves. The input node stress on the bottom boundary of the model is given by the following formulas

$$\begin{cases} F_{BS}^T = k_T u_{rs} + c_T \dot{u}_{rs} + \rho c_s \dot{u}_{rs} \\ F_{BS}^N = 0 \\ F_{BS} = F_{BS}^T + F_{BS}^N \end{cases} \tag{3}$$

The input node stress on the lateral boundaries of the model is as follows

$$\begin{cases} F_{SS}^T = \pm \rho c_s \dot{u}_{fs} \\ F_{SS}^N = k_N u_{fs} + c_N \dot{u}_{fs} \\ F_{SS} = F_{SS}^T + F_{SS}^N \end{cases} \tag{4}$$

where F_{BS}^T, F_{BS}^N, and F_{BS} are the tangential, normal, and total input node stresses on the bottom boundary of the model under shear wave action, respectively; F_{SS}^T, F_{SS}^N, F_{SS} are the tangential, normal, and total input node stresses on the lateral boundaries of the model under shear wave action, respectively; u_{rs} and $\dot{u}_{rs}$ are the displacement and velocity of the shear wave, respectively; and u_{fs} and $\dot{u}_{fs}$ are the displacement and velocity caused by the propagating shear wave in free strata, respectively.

According to the acceleration time history curves in the E-W and N-S directions, the respective input node stresses in the single direction were calculated. For the E-W motion, the lateral boundaries that experienced node stress were on the left and right boundaries of the model. The tangential input node stress on one boundary was $\rho c_s \dot{u}_{fs}$ and that on the other was $-\rho c_s \dot{u}_{fs}$. For the N-S motion, the lateral boundaries that experienced node stress were on the front and back boundaries of the model. Similarly, the input node-stress values on both boundaries were equal, with one being positive and the other negative.

Compression waves, which travel vertically upward from the bottom of the model, can cause model particles to vibrate up and down. The input node stress on the bottom boundary of the model is given by the following formulas

$$\begin{cases} F_{BP}^T = 0 \\ F_{BP}^N = k_N u_{rp} + c_N \dot{u}_{rp} + \rho c_p \dot{u}_{rp} \\ F_{BP} = F_{BP}^T + F_{BP}^N \end{cases} \tag{5}$$

The input node stress on the lateral boundaries of the

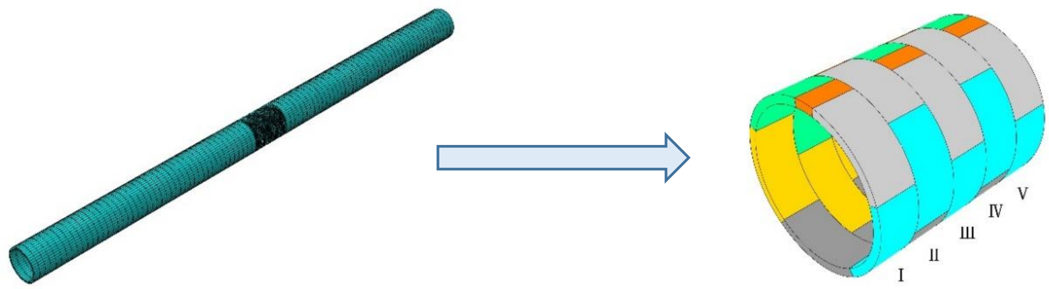

(a) Lining structure (b) Assembled structure of five segmental lining rings

Fig. 6 Tunnel lining structure

model is as follows

$$\begin{cases} F_{SP}^{T} = k_T u_{fp} + c_T \dot{u}_{fp} \\ F_{SP}^{N} = \frac{\lambda}{\lambda+2G} \rho c_p \dot{u}_{fp} \\ F_{SP} = F_{SP}^{T} + F_{SP}^{N} \end{cases} \tag{6}$$

where F_{BP}^{T}, F_{BP}^{N}, and F_{BP} are the tangential, normal, and total input node stresses on the bottom boundary of the model under compression wave action, respectively; F_{SP}^{T}, F_{SP}^{N}, and F_{SP} are the tangential, normal, and total input node stresses on the lateral boundaries of the model under compression wave action, respectively; u_{rp} and $\dot{u}_{rp}$ are the displacement and velocity of the compression wave, respectively; and u_{fp} and $\dot{u}_{fp}$ are the displacement and velocity caused by the propagating compression wave in free strata, respectively.

The total stress input to the model boundary is the sum of the boundary input stress caused by shear and compression waves, and the formula is as follows

$$\begin{cases} F_B = F_{BS} + F_{BP} \\ F_S = F_{SS} + F_{SP} \end{cases} \tag{7}$$

Considering the reflection of the seismic wave on the free surface, the actual input node stress on the bottom boundary of the model is given by the following formula

$$F_B(t) = F_B(t) + F_B\left(t - \frac{2h}{c}\right) \tag{8}$$

The actual input node stress on the lateral boundaries of the model is as follows

$$F_S(t) = F_S\left(t - \frac{l}{c}\right) + F_S\left(t - \frac{2h-l}{c}\right) \tag{9}$$

where $F_B(t)$ and $F_S(t)$ are the actual input node stresses on the bottom and lateral boundaries of the model at moment *t*, respectively; *h is* the height of the model; *l* is the distance from the node on the lateral boundary to the bottom boundary; and *c* is the propagation velocity of the seismic waves.

3.3 Assembled segmental lining

Seismic dynamic response analysis requires extremely high computational performance. Rather than reducing the computational efficiency by refining the simulation of all the segmental linings, the middle of tunnel lining was simulated based on the assembled structure of five segmental lining rings (I-V) and the rest was simulated using a homogenous ring based on the equivalent principle of flexural rigidity (Yan *et al*. 2017, 2018a, b), as shown in Fig. 6.

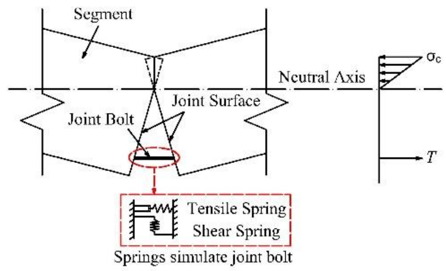

Fig. 7 Mechanical model of segmental joint

To form a segmental lining, prefabricated reinforced concrete segments are connected by circumferential and longitudinal bolts. From the structural perspective, a segmental joint of adjacent segments mainly comprises joint surfaces and joint bolts. The tensile resistance of a segmental joint is determined by the joint bolt, whereas the compressive resistance of a segmental joint is mainly determined by the joint surface. In addition, the shear and flexural resistances are determined by both the joint surface and joint bolt. A mechanical model of a segmental joint was built, as shown in Fig. 7, in which *T* is the tensile force on the segmental joint bolt and σ_c is the pressure on the segmental joint surface. Based on the above analysis, the contact surface was used to simulate the segmental joint surface and a tensile spring and shear spring together were used to simulate a segmental joint bolt. In this study, the tensile and shear spring stiffness values were 2.33×10^8 N/m and 5.97×10^7N/m, respectively.

The contact relationship in the model is shown in Fig. 8. The interaction between segmental lining and surrounding strata adopted surface-to-surface contact; hard contact was applied in the normal direction, which transmits contact pressure between the contact surfaces and allows the contact surfaces to separate, and coulomb friction was applied in the tangential direction. Surface-to-surface contact was also applied between segments; hard contact was applied in the normal direction and coulomb friction was applied in the tangential direction. The formula for the coulomb friction is as follows

$$\tau = \mu P \tag{10}$$

where τ is the critical shear stress and μ is the friction

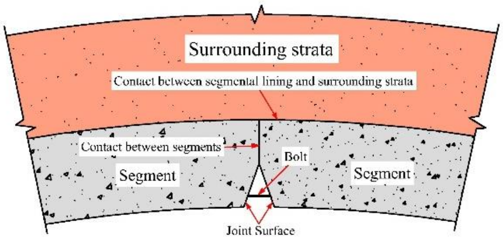

Fig. 8 Contact relationship

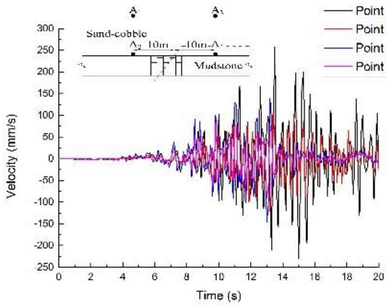

Fig. 9 Velocity time-history curves of analysis points A_1-A_4

coefficient. In this paper, the contact between segments was set at μ=0.6 and for the contact between the segmental lining and surrounding strata, μ=0.8 (Yan *et al.* 2016), where P is the normal contact pressure between the contact surfaces.

Based on the equivalent principle of flexural rigidity, the rest of the tunnel lining was approximately simulated by reducing the overall flexural rigidity. The equivalent flexural rigidity equations are as follows (Koizumi 2012)

$$(EI)_{eq} = \frac{cos^3\varphi}{cos\varphi+\left(\frac{\pi}{2}+\varphi\right)sin\varphi} E_s I_s \tag{11}$$

$$\varphi + cot\varphi = \pi(0.5 + \frac{K_J}{E_S A_S / l_S}) \tag{12}$$

where φ is the angle between the neutral axis and the horizontal line at the center of tunnel; E_s and A_s are the elastic modulus of the tunnel lining and the cross-section area of the tunnel, respectively; $A_s = \pi(D^2 - d^2)/4$, D and d are the external and internal diameters of the shield tunnel, respectively; the moment of inertia of the ring section $I_s = \pi(D^4 - d^4)/64$; the bolt tensile stiffness $K_J = n \times k_j$, k_j is the tensile stiffness of a single bolt, n is the number of longitudinal bolts between the segmental lining rings; and l_s is the width of the segmental lining ring. The equivalent flexural rigidity of the tunnel lining was calculated to be 3.7×10^7 kN·m^2.

4. Results analysis and discussion

In this section, the tunnel-strata numerical model used in dynamic analysis is presented and the ground velocity, the acceleration, displacement, additional principal stress, and joint deformation of the segmental lining in response to the Wenchuan earthquake are analyzed.

4.1 Ground velocity

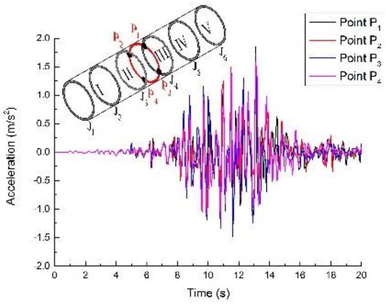

(a) Acceleration

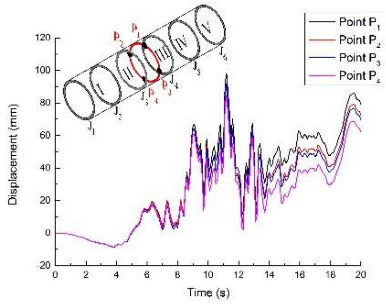

(b) Displacement

Fig. 10 East-west acceleration and displacement time-history curves of analysis points P_1-P_4

The east-west velocity of the analysis points were obtained and plotted as time history curves, as shown in Fig. 9. Analysis points A_2 and A_4 are located at the tunnel arch in the sand-cobble layer and mudstone layer respectively, 10 m away from the interface between the sand-cobble and mudstone layers, and analysis points A_1 and A_3 are on the surface, directly above analysis points A_2 and A_4, respectively. As shown in the figure, at the same time the velocity of analysis point A_1 is faster than that of analysis point A_3, and the velocity of analysis point A_2 is faster than that of analysis point A_4. The velocity time-history curves of analysis points A_1-A_4 reached their maximums in 13.5 s, 13.4 s, 13.2 s, and 13.2 s, at 285 mm/s, 108 mm/s, 139 mm/s, and 81 mm/s, respectively. The velocity response of analysis point A_2 is stronger than that of analysis point A_4, which forms a difference in dynamic response between the two sides of the interface. And the difference in dynamic response will cause segmental joint opening and dislocation.

4.2 Acceleration, displacement, and additional principal stress of the segmental lining

The analysis points P_1, P_2, P_3, and P_4 are located at the top, left, right, and bottom of the middle section of segmental lining ring III, respectively. The east-west acceleration and displacement of the analysis points were obtained and plotted as time history curves, as shown in Fig. 10. As shown in the figure, the acceleration change trends of the analysis points were essentially identical, as were their displacements. The acceleration time-history curves of analysis points P_1-P_4 reached their maximums in 13.1 s, at 1.85 m/s^2, 1.72 m/s^2, 1.69 m/s^2, and 1.59 m/s^2, respectively. Compared with the maximum east-west input

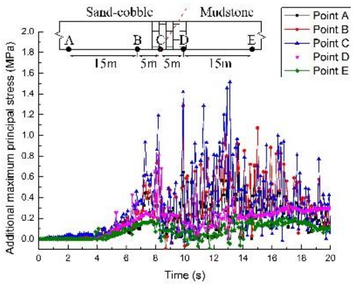

Fig. 11 Additional maximum principal stress time-history curves of analysis points A-E

seismic acceleration, the maximum accelerations of analysis points P_1-P_4, were greater by about 1.9, 1.8, 1.8, and 1.7 times, respectively, and their displacement time-history curves reached their maximums in 11.2s at 98.1 mm, 91.9 mm, 91.6 mm and 84.6 mm, respectively. Regarding the displacements of the analysis points at the same moment, P_1 had the maximum value, followed by P_2 and P_3, and P_4 with the minimum. These results show that the closer the point was to the ground, the greater were its acceleration and displacement responses.

Fig. 11 shows a plot of the additional maximum principal stress time-history curves of analysis points A-E. Analysis point C is located at the tunnel arch bottom at the interface between the sand-cobble and mudstone layers. Analysis points A and B are located at the tunnel arch bottom in the sand-cobble layer at distances from point C of 20 m and 5 m, respectively, whereas analysis points D and E are located at the tunnel arch bottom in the mudstone layer at distances from point C of 5 m and 20 m, respectively. From Fig. 10, it is evident that the maximum value of the additional maximum principal stress of point C was 1.51 MPa; the maximum value of the additional maximum principal stress of points A and B were 0.91 MPa and 1.28 MPa, respectively, and the maximum value of the additional maximum principal stress of points D and E were 0.80 MPa and 0.23 MPa, respectively. The additional maximum principal stress of point C at the stratigraphic interface was found to be the largest. As the distance from the stratigraphic interface increased, the additional maximum principal stress of the corresponding analysis point decreased. Furthermore, the additional maximum principal stress of the tunnel arch bottom in the looser sand-cobble layer was greater than that at the corresponding position in the mudstone layer, such as at points B and D and points A and E.

4.3 Segmental joint deformation

Shield tunnel lining is manufactured in assembly segments with circumferential and longitudinal joints. Openings and dislocations can occur in segmental joints subjected to earthquake action. Fig. 12 shows a magnified display of a segmental joint opening and dislocation subjected to earthquake action.

Table 2 lists the maximum opening and dislocation of a circumferential joint subjected to earthquake action, in which it can be seen that the maximum opening and

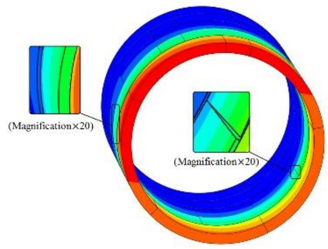

Fig. 12 Magnification of an opening and dislocation in a segmental joint

Table 2 Maximum openings and dislocations of circumferential joints

Circumferential joint	Maximum opening /mm	Maximum dislocation /mm	Schematic diagram
J_1	10.1	5.2	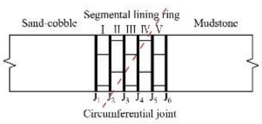
J_2	13.3	13.8	
J_3	15.3	18.3	
J_4	8.7	8.6	
J_5	5.3	2.1	
J_6	2.4	0.8	

dislocation of circumferential joint J_3 were the largest of circumferential joints J_1-J_6, whereas those of circumferential joint J_6 were the smallest. The relationships between the circumferential joints in the sand-cobble layer with respect to the maximum opening and dislocation was $J_2>J_1$, whereas the relationship between those in the mudstone layer was $J_3>J_4>J_5>J_6$. This can be explained by the fact that a larger relative deformation occurred at the interface between the soft and hard layers subjected to earthquake action and the farther the circumferential joint was from the interface, the smaller was its deformation. Moreover, the openings and dislocations of the circumferential joints in the sand-cobble layer were larger than those in the mudstone layer subjected to earthquake action due to the greater seismic deformation of the sand-cobble layer.

The details of opening and dislocation of circumferential joint J_3 was analyzed further. The analysis points O_1, O_2, O_3, and O_4 are located at the top, left, right, and bottom of circumferential joint J_3, respectively, at a distance of $t/3$ from the outer surface of the segmental lining (t is the segment thickness), which approximately corresponds with the location of the elastic sealing gasket on the segmental joint. Fig. 13 shows a plot of the joint-opening time-history curves of analysis points O_1-O_4, in which it is evident that all the curves reached their maximum in 9.0s, at 12.5 mm, 15.3 mm, 12.8 mm, and 10.6 mm, respectively. The maximum opening of circumferential joint J_3 occurred on the left of the circumferential joint.

To investigate the contribution of single-directional motion to an opening in a circumferential joint, the numerical calculation was performed only inputting the E-W, N-S, and U-D seismic motions. Fig. 14 shows plots of the joint-opening time-history curves of analysis points O_1-O_4 under single-directional motion. As can be seen in the

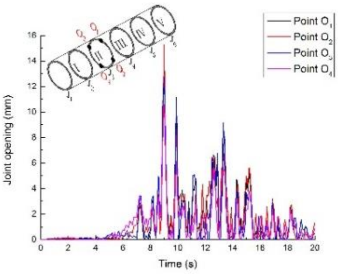

Fig. 13 Joint-opening time-history curves of analysis points O_1-O_4

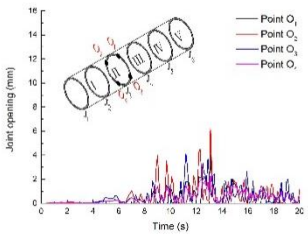

(a) Only E-W motion

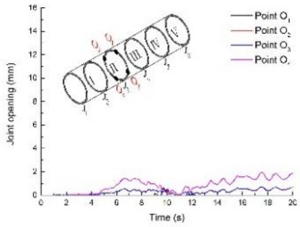

(b) Only U-D motion

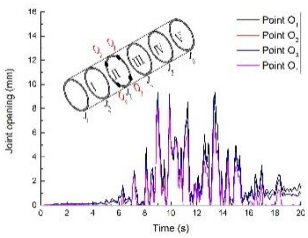

(c) Only N-S motion

Fig. 14 Joint-opening time-history curves of analysis points O_1-O_4 under single-direction motion

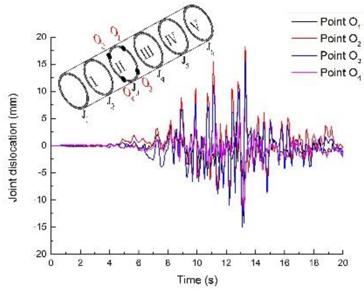

Fig. 15 Joint-dislocation time-history curves of analysis points O_1-O_4

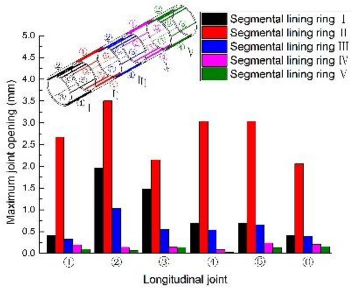

(a) Joint openings

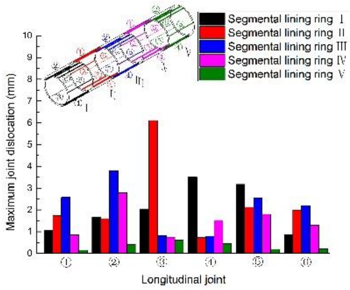

(b) Joint dislocations

Fig. 16 East-west acceleration and displacement time-history curves of analysis points P_1-P_4

figure, when only the seismic motion of a single direction was input, the relative sizes of the joint J_3 opening caused by the three motion directions are as follows: N-S motion>E-W motion>U-D motion. The contributions of the single-direction motions along the longitudinal, horizontal, and vertical directions of the tunnel to the opening of circumferential joint J_3 were approximately 60%, 30%, and 10%, respectively, of the combined three-directional motion. These results indicate that the opening of circumferential joint J_3 was mainly caused by motion along the tunnel, whereas the motions across the tunnel in both directions contributed only slightly.

Fig. 15 shows a plot of the joint-dislocation time-history curves of analysis points O_1-O_4 of the combined three-directional motion. From the figure, it is evident that the joint-dislocation time-history curves of analysis points O_1 and O_4 reached their maximum in 13.2 s, at −14.3 mm and −12.0 mm, respectively, and those of analysis points O_2 and O_3 reached their maximum in 13.3 s, at 18.3 mm and 15.8 mm, respectively. The times of maximum dislocation at four typical locations were very close. In addition, the change trends of the dislocations of points O_1 and O_4 were essentially in agreement, as were points O_2 and O_3. This can be explained by the fact that the segmental lining, as a non-rigid body, deformed to a certain extent due to earthquake action, so the joint dislocations of points O_1 and O_4 or points O_2 and O_3 at the same time were not exactly the same. Also, the joint dislocations of points O_2 and O_3 were larger than those of points O_1 and O_4, due to the greater intensity of the E-W motion than the U-D motion.

There are more longitudinal joints than circumferential joints in segmental lining rings I−V. To determine the openings and dislocations of longitudinal joints of a segmental lining subjected to earthquake action, the maximum joint openings and dislocations of the longitudinal joints of segmental lining rings I−V were obtained, as shown in Fig. 16.

Fig. 16(a) shows the maximum joint openings of the longitudinal joints of segmental lining rings I−V. From the figure, it is evident that a maximum joint opening of 3.5 mm occurred at longitudinal joint ② of segmental lining ring II, and that the relationship of the maximum openings of the longitudinal joints in the sand-cobble layer was II>I and in the mudstone layer was III>IV>V. Fig. 16(b) shows the maximum joint dislocations of the longitudinal joints in segmental lining rings I−V. As shown in the figure, a maximum joint dislocation of 6.1 mm occurred at longitudinal joint ③ of segmental lining ring II, and the

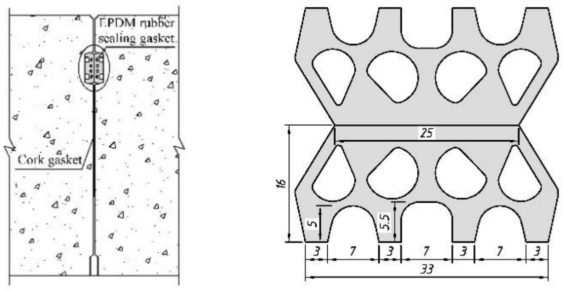

(a) Joint waterproof structure
(b) Cross-section schematic of EPDM sealing gasket (mm)

Fig. 17 Segmental joint waterproof structure

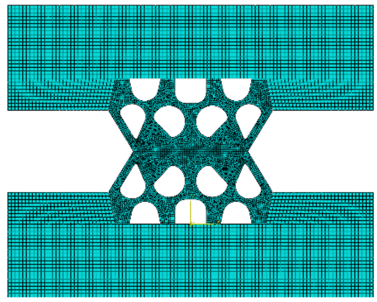

Fig. 18 Numerical model for waterproof property

maximum dislocations of the other longitudinal joints were less than 4 mm. The distribution of the maximum openings of the longitudinal joints was basically consistent with that of the maximum joint dislocation of the segmental lining rings I-V.

As determined by the above analysis, the joint openings and dislocations of circumferential joints are much larger than those of longitudinal joints. As such, the circumferential joint is considered to be the control joint for structurally waterproofing shield tunnels subjected to earthquake action. The analysis results indicate that the least favorable situations with respect to segmental joint deformation in this section of the shield tunnel subjected to the Wenchuan earthquake are as follows: joint opening of 15.3 mm and joint dislocation of 6.6 mm (at point O_2); joint opening of 6.4 mm and joint dislocation of 18.3 mm (at point O_2). Therefore, it is necessary to analyze the waterproof property of the elastic sealing gasket in this section of the shield tunnel and determine its waterproof effectiveness in these unfavorable situations.

5. Verification of segmental lining waterproof property after joint deformation

Existing research indicates that the opening and dislocation deformation of segmental joints can alter the waterproofing property. In this study, both numerical simulation and laboratory tests were used to analyze the waterproof property in the above unfavorable situations. Focusing on the elastic sealing gasket in the shield tunnel of Line 1 of the Chengdu Metro, a numerical analysis of the contact pressure along the seepage path was conducted and the waterproof property of the elastic sealing gasket under different joint openings and dislocations investigated. In Line 1 of the Chengdu Metro, EPDM sealing gaskets are installed in the segmental sealing groove on circumferential and longitudinal joints to realize a waterproof segmental lining joint, as shown in Fig. 17. The caulking grooves of China's urban metro tunnels are not generally filled, the effect of filler in the caulking groove were not considered in our analysis of waterproof property.

5.1 Numerical model for waterproof property

As EPDM is hyperelastic, the Mooney-Rivlin constitutive model is often adopted in its numerical simulation. The strain-energy density function W of this model can be expressed as follows

$$W = C_{10}(I_1 - 3) + C_{01}(I_2 - 3) \tag{13}$$

where W is the strain-energy density function; I_1 and I_2 are the first and second Green strain invariants, respectively; and C_{10} and C_{01} are the material constants of the Mooney-Rivlin model.

Due to the incompressibility of rubber (Poisson's ratio v=0.5), the relationship of the shear modulus G, elastic modulus E, C_{10}, and C_{01} is as follows

$$G = \frac{E}{2(1+v)} = \frac{E}{3} = 2(C_{10} + C_{01}) \tag{14}$$

Gent (2001) suggested that a C_{01}/C_{10}=0.25 was reasonable in the Mooney-Rivlin model. Substituting this value into Formula (14), the Formula (15) is obtained

$$E = 6(C_{10} + 0.25C_{10}) \tag{15}$$

According to rubber test data, the following relationship between the rubber hardness H and the elastic modulus E is obtained (Gent 2001)

$$E = \frac{15.72+2.15H}{100-H} \tag{16}$$

In this paper, the rubber hardness H of the elastic sealing gasket is 50. The material constant C_{10} and C_{01} were calculated to be 0.329 MPa and 0.082 MPa, respectively. As the cross-sectional size of the elastic sealing gasket is much smaller than its longitudinal size, a plane strain model was developed for the waterproof analysis, as shown in Fig. 18. Four-node plane strain quadrilateral elements (CPE4) were used to simulate the elastic sealing gaskets and segmental lining. There were 9,770 elements in the numerical model. The Mooney-Rivlin constitutive model was considered for the elastic sealing gaskets, while the elastic constitutive model was adopted for the segmental lining. Fixed boundaries were set at the bottom of the model. Friction contact was applied between the elastic sealing gaskets and between the elastic sealing gaskets and segmental sealing groove, and self-contact was applied on the surfaces of the internal holes of the elastic sealing gaskets.

5.2 Numerical analysis of waterproof property

Fig. 19 shows plots of the von Mises stress of the elastic sealing gasket under different joint openings for a joint dislocation of 0 mm. From this figure, it is evident that

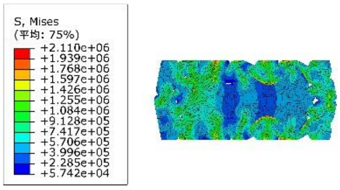

(a) Joint opening 0 mm

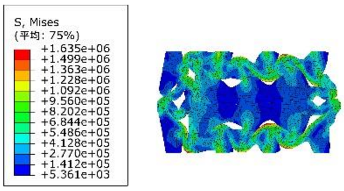

(b) Joint opening 4 mm

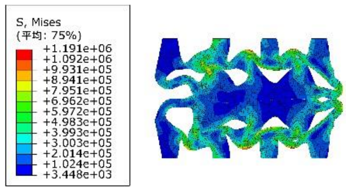

(c) Joint opening 8 mm

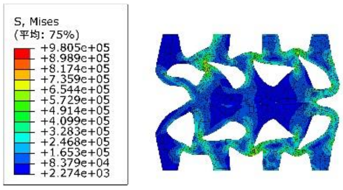

(d) Joint opening 12 mm

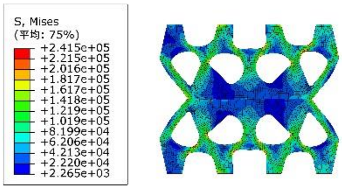

(e) Joint opening 16 mm

Fig. 19 Von Mises stress of elastic sealing gaskets with different joint openings for a joint dislocation of 0 mm

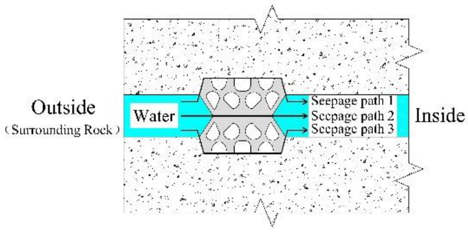

Fig. 20 Seepage paths of the elastic sealing gasket

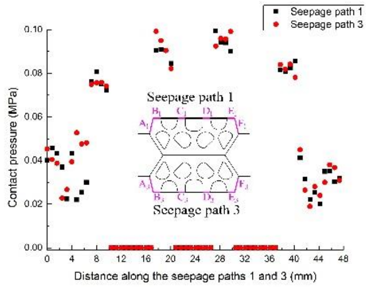

(a) Along seepage paths 1 and 3

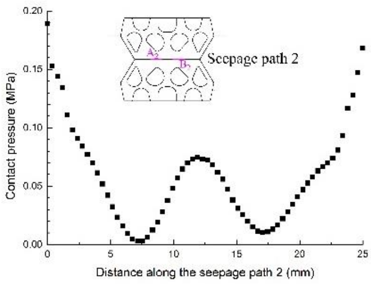

(b) Along seepage path 2

Fig. 21 Contact pressure along three seepage paths when joint opening is 14 m and dislocation is 0 m

when the joint opening was 0 mm, the segmental sealing groove well was filled by the elastic sealing gasket and the entire elastic sealing gasket had a large deformation. When the joint openings were 0 mm, 4 mm, 8 mm, 12 mm, and 16 mm, the maximum von Mises stress of the elastic sealing gaskets were 2.11 MPa, 1.64 MPa, 1.19 MPa, 0.98 MPa, and 0.24 MPa, respectively. This shows that with the increasing joint openings, holes in the elastic sealing gaskets gradually opened and the maximum von Mises stress gradually decreased. Note that all the maximum von Mises stresses occurred around the holes of the elastic sealing gaskets. This can be explained by the fact that the parts of the elastic sealing gasket that can undergo a large deformation are primarily the holes in the confined space of the segmental sealing groove.

Regardless of the destruction and deterioration of the elastic sealing gasket, the water enters the tunnel only along the contact surfaces between the elastic sealing gaskets or between elastic sealing gasket and the segmental sealing groove, as shown in Fig. 20. The contact pressure between elastic sealing gaskets, and between elastic sealing gasket and the segmental sealing groove can determine the waterproof property of the elastic sealing gasket. The seepage path, along which the maximum contact pressure is minimum among three seepage paths, is regarded as the control path. The maximum water pressure that the elastic sealing gasket can withstand is the maximum contact pressure along the control path. Once the external water pressure is greater than the maximum contact pressure along the control path, the elastic sealing gasket can no longer prevent water from seeping in.

Fig. 21 shows plots of the contact pressures along three seepage paths for a joint opening of 14 mm and a dislocation of 0 mm. As shown in the figure, the distributions of the contact pressure along seepage paths 1 and 3 are basically symmetrical. In addition, the contact pressure in contact areas C and D was the greatest, that in contact areas B and E was next, and that in contact areas A and F was the least. The contact pressure in the areas corresponding to the holes was 0 MPa. The peak of the contact pressure along seepage path 1 was 0.0995 MPa, which occurred in contact area D_1, whereas that along seepage path 3 was 0.0992 MPa, which occurred in contact area C_3. Note that the contact-pressure peaks along seepage paths 1 and 3 differ slightly. It is speculated that this slight difference is due to calculation error. Along seepage path 2, the contact pressure presents a “W” distribution. Contact areas A_2 and B_2, in which the contact pressures were relatively small, were located between two semicircular

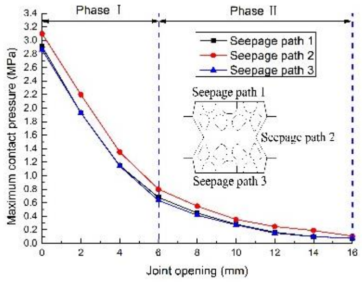

Fig. 22 Change curves of maximum contact pressures along three seepage paths with different size joint openings when dislocation is 0 mm

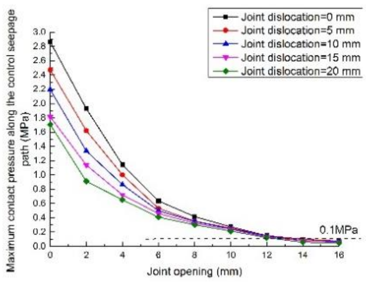

Fig. 23 Maximum contact pressure along the control seepage path under different joint openings and dislocations

holes in the middle of the upper and lower elastic sealing gaskets. This can be explained by the fact that when the elastic sealing gasket was greatly deformed, the holes closed and absorbed much of the deformation energy, which caused the contact pressure between the two semicircular holes to decrease. The contact-pressure peak along seepage path 2 was 0.1891 MPa. Neglecting calculation error, the contact pressure along seepage paths 1 and 3 was the least. Therefore, seepage paths 1 and 3 were the control paths. This analysis reveals that the waterproof property of the elastic sealing gasket was 0.0992 MPa when the joint opening was 14 mm and dislocation was 0 mm.

Fig. 22 shows plots of the curves of the maximum contact pressures of three seepage paths with different joint openings for a dislocation of 0 mm. From the figure, it is evident that the maximum contact pressures on the three seepage paths decreased with increases in the joint opening. The maximum-contact-pressure-joint-opening relationship can be divided into two phases. In phase Ⅰ, the joint openings range in size from approximately 0 mm to 6 mm, and the observed maximum contact pressure decreases rapidly as the joint opening increases in size. In phase Ⅱ, the joint openings range in size from 6 mm to 16 mm, and the maximum contact pressure decreases slowly as the size of the joint opening increases. This can be explained by the fact that when the joint opening is small, there is an obvious rebound deformation of the elastic sealing gasket as the joint opens. However, once the joint has opened to a certain extent, this rebound deformation of the elastic sealing gasket is no longer evident as the joint opening size continues to increase. Of the three seepage paths, the maximum contact stress along the seepage path 2 is the highest and those of seepage paths 1 and 3 were basically the same. These results show that when the joint dislocation was 0 mm, seepage paths 1 and 3 were the control paths no matter how large the joint opening becomes, and the maximum waterproof property of the elastic sealing gasket is determined by the maximum contact pressures of seepage paths 1 and 3.

Fig. 23 shows the maximum contact pressure along the control seepage path under different joint openings and

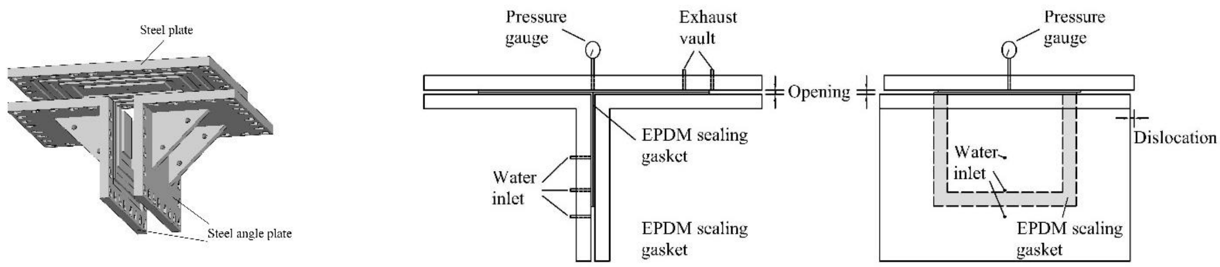

(a) Test device (b) Test principles

Fig. 24 Schematic diagram of test device and test principles

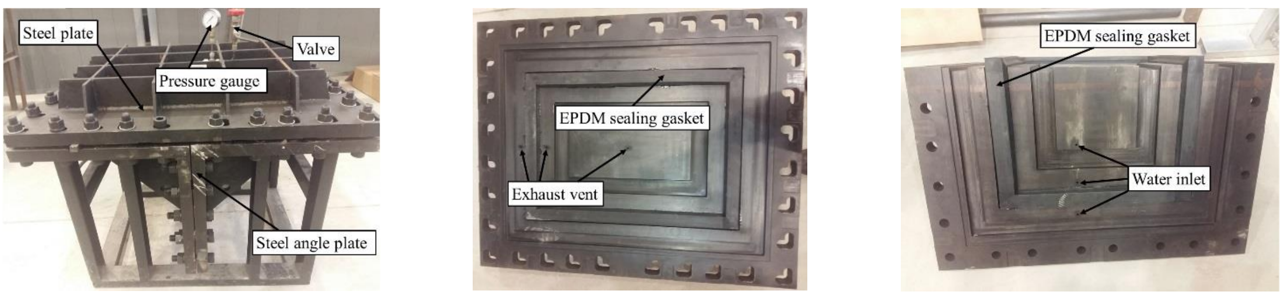

(a) Entire device (b) Steel plate (c) Steel angle plate

Fig. 25 Test device

dislocations. As shown in this figure, the maximum contact pressure along the control seepage path decreased as the size of the joint opening increased when the joint dislocation did not change. When the joint opening was less than 10 mm, the maximum contact pressure along the control seepage path decreased as the joint dislocation increased. However, the joint dislocation had little influence on the maximum contact pressure along the control seepage path when the joint opening was larger than 10 mm. In actual projects, the cork gasket is often set on the segmental joint to prevent extrusion of the segmental joint surface. Therefore, a joint opening of approximately 2-3 mm always remains after the normal assembly of segments. As such, a joint opening of 0 mm is simply an ideal state. In actual projects, the maximum water property of a shield tunnel is often not more than about 1.6 MPa.

Based on the shield tunnel passing through soft-hard inhomogeneous layers on Line 1 of the Chengdu Metro, the water leakages in the least favorable situations of segmental joint deformation subjected to earthquake action (joint opening of 15.3 mm and joint dislocation of 6.6 mm; joint opening of 6.4 mm and joint dislocation of 18.3 mm) were analyzed. Given a water head of 10 m, water leakage will appear in the former scenario but not in the latter. The analysis results indicate that water leakage appeared at the left of the circumferential joint in the section of the shield tunnel passing through the interface between the sand-cobble and mudstone layers, which was consistent with the observed earthquake damage.

5.3 Test verification of waterproof property

Using the segmental joint deformation obtained from numerical analysis of the seismic response, a waterproof test of the elastic sealing gasket was conducted to verify the occurrence of water leakage in the most unfavorable segmental joint deformations in the shield tunnel. Fig. 24 shows the test device and the principles of the waterproof test.

The waterproof test device mainly comprised steel templates, a hydraulic pump, pressure gauges, valves, and steel bolts, as shown in Fig. 25. The steel templates consisted of a steel plate and two steel angle plates, with the dimensions 800 mm×600 mm and 600 mm×400 mm×400 mm, respectively. The thickness of the steel templates is 36 mm. Three sealing grooves were machined in every steel template corresponding to the three different cross-sectional elastic sealing gaskets. Then, three holes were drilled on the steel plate as exhaust-vent and pressure measurement holes and three holes on the steel angle plate as water inlets.

The joint opening of the test device was controlled by adding shims of different thicknesses between the steel plate and steel angle plate, and the degree of joint dislocation was modified by moving the steel plate. Bolts were used to fix the device, thereby preventing any change in the joint opening and dislocation during the test. At the beginning of the test, the hydraulic pump and pressure gauges were connected to the device and then water was poured into the test device until it flowed out of the exhaust vent, indicating that there was no longer air in the device. Then, close the exhaust vent valve and keep the water

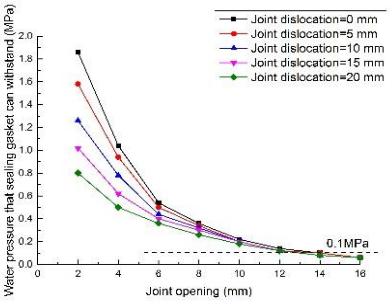

Fig. 26 Water pressure that elastic sealing gasket can withstand under different joint openings and dislocations

pressure stable at an initial small water pressure of 0.04 MPa for 20 minutes. Then the water pressure was increased in 0.02 MPa increments. After every addition, this water pressure was maintained for 10 minutes. If there was no leakage, the pressure continued to be increased. If leakage occurred, the elastic sealing gasket was considered to be no longer waterproof at this water pressure and the effective waterproof property of the elastic sealing gasket were the water pressures before this water pressure was increased 0.02 MPa.

Fig. 26 shows the water pressure that elastic sealing gasket can withstand under different joint openings and dislocations. From the figure, it is evident that when the joint dislocation remained unchanged, the water pressure that elastic sealing gasket can withstand decreased as the joint opening increased and the decrement decreased as the joint opening increased. When the joint opening was less than 10 mm, the water pressure that elastic sealing gasket can withstand obviously decreased as the joint dislocation increased. However, joint dislocation had little effect on the water pressure that elastic sealing gasket can withstand when the joint opening was larger than 10 mm. This test result basically accords with our numerical simulation result.

The waterproof test results indicate that, given a water head of 10 m, water leakage will occur with a joint opening of 15.3 mm and a joint dislocation of 6.6 mm, but no water leakage will occur when the joint opening is 6.4 mm and joint dislocation is 18.3 mm. This waterproof test result basically agrees with our numerical simulation result, therefore verifying again the actual water leakage due to damage from the Wenchuan earthquake to the shield tunnel in Line 1 of the Chengdu Metro. This shows that the influences of joint opening and dislocation caused by earthquake action on the waterproof property of elastic sealing gaskets should be fully considered in the aseismic design of shield tunnels.

6. Conclusions

Based on the section of the shield tunnel in Line 1 of the Chengdu Metro that passes through the interface between sand-cobble and mudstone layers, a 3D model of a shield tunnel with an assembled segmental lining was built for the purpose of analyzing the dynamic response of the segmental lining and the deformation of the segmental joints. Numerical simulations and laboratory tests were conducted to analyze the waterproof property of the elastic sealing gasket used in the shield tunnel. The following are the main conclusions obtained from the research:

- Compared with the conventional seismic-motion input method that inputs acceleration, the node-stress input method has good adaptability to seismic analysis. This method considers the seismic motion of the lateral boundary nodes and the reflection of seismic wave on the free surface and fits well with the viscous-spring artificial boundary.
- The contact surface and a spring were used to simulate the segmental joint surface and joint bolt. Respectively, the tensile, compressive, shear, and flexural resistances of the segmental joint were obtained. While reducing the required computing power, the structural analysis model of the shield tunnel developed by combining a partially refined model of the assembled segmental lining with a model of its structural equivalent flexural rigidity, also has good adaptability for analyzing the dynamic response of the shield tunnel, especially with respect to joint openings and dislocations.
- For shield tunnels passing through the interface of soft-hard inhomogeneous strata, the acceleration, displacement and joint deformation of segmental linings are subject to significant earthquake action. As the distance from the interface increases, the structural dynamic response decreases. Compared with the looser sand-cobble layer, there is a smaller structural dynamic response of the shield tunnel in the corresponding position in the mudstone layer.
- For shield tunnels passing through the interface of soft-hard inhomogeneous strata, the joint openings and dislocations of circumferential joints are always much greater than those of longitudinal joints. The opening of circumferential joints is mainly caused by motion along the tunnel, but motion along the tunnel cross section in the horizontal and vertical directions contributes only slightly.
- Joint openings and dislocations both affect the waterproof property of the elastic sealing gasket. For the shield tunnel on Line 1 of the Chengdu Metro, when the joint dislocation remains unchanged, the waterproof property of the elastic sealing gasket decreases rapidly as the joint opening increases until the joint opening reaches 6 mm, after which its waterproof property decreases slowly as the joint opening increases. When the joint opening is less than 10 mm, the waterproof property of the elastic sealing gasket obviously decreases as the joint dislocation increases. When the joint opening is larger than 10 mm, joint dislocation has little influence on the waterproof property.

In this paper, based on the analysis of joint deformation in the shield tunnel on Line 1 of the Chengdu Metro subjected to earthquake action and an investigation of the waterproof property of the elastic sealing gasket, the inevitability of water leakage at the arches of circumferential joints in the shield tunnel passing through the interface between sand-cobble and mudstone layers during the 2008 Wenchuan earthquake was verified. There were a number of deficiencies in this study that should be noted, as follows: (1) The influence of bolt fracture on the joint openings was not taken into account. (2) Only the joint openings and dislocations caused by earthquake action were considered, and any initial deformations of segmental joints caused by assembly error were neglected. (3) In the analysis of the waterproof property of the elastic sealing gasket, the deformation of the joint opening were considered to be uniform and any differences in the joint opening on the outside and inside of segments with respect to segmental thickness were ignored.

Acknowledgments

Financial support for this work provided by the National Key R & D Program of China (Grant no.2016YFC0802205), and the National Science Foundation of China (Grant no.51678500) is gratefully acknowledged.

References

Amorosi, A. and Boldini, D. (2009), "Numerical modelling of the transverse dynamic behaviour of circular tunnels in clayey soils", *Soil Dyn. Earthq. Eng.*, **29**(6), 1059-1072. https://doi.org/10.1016/j.soildyn.2008.12.004.

Balendra, T., Thambiratnam, D.P., Koh, C.G. and Lee, S.L. (1984), "Dynamic response of twin circular tunnels due to incident SH-waves", *Earthq. Eng. Struct. Dyn.*, **12**(2), 181-201. https://doi.org/10.1002/eqe.4290120204.

Ding, J.H., Jin, X.L., Guo, Y.Z. and Li, G.G. (2006), "Numerical simulation for large-scale seismic response analysis of immersed tunnel", *Eng. Struct.*, **28**(10), 1367-1377. https://doi.org/10.1016/j.engstruct.2006.01.005.

Ding, W.Q., Gong, C.J., Mosalam, K.M. and Soga, K. (2017), "Development and application of the integrated sealant test apparatus for sealing gaskets in tunnel segmental joints", *Tunn. Undergr. Sp. Tech.*, **63**, 54-68. https://doi.org/10.1016/j.tust.2016.12.008.

Fabozzi, S. and Bilotta, E. (2016), "Behaviour of a segmental tunnel lining under seismic actions", *Procedia Eng.*, **158**, 230-235. https://doi.org/10.1016/j.proeng.2016.08.434.

Fattah, M.Y., Hamoo, M.J. and Dawood, S.H. (2015), "Dynamic response of a lined tunnel with transmitting boundaries", *Earthq. Struct.*, **8**(1), 275-304. http://dx.doi.org/10.12989/eas.2015.8.1.275.

Gent, A.N. (2001), *Engineering With Rubber: How to* Design *Rubber Components*, Hanser Gardner Publications Inc., Cincinnati, Ohio, USA.

Gomes, R.C., Gouveia, F., Torcato, D. and Santos, J. (2015), "Seismic response of shallow circular tunnels in two-layered ground", *Soil Dyn. Earthq. Eng.*, **75**, 37-43. https://doi.org/10.1016/j.soildyn.2015.03.012.

Guo, Y., Jin, X. and Ding, J. (2006), "Parallel numerical simulation with domain decomposition for seismic response analysis of shield tunnel", *Adv. Eng. Softw.*, **37**(7), 450-456. https://doi.org/10.1016/j.advengsoft.2005.09.008.

Hashash, Y.M., Hook, J.J., Schmidt, B., John, I. and Yao, C. (2001), "Seismic design and analysis of underground structures", *Tunn. Undergr. Sp. Tech.*, **16**(4), 247-293. https://doi.org/10.1016/S0886-7798(01)00051-7.

Hatzigeorgiou, G.D. and Beskos, D.E. (2010), "Soil-structure interaction effects on seismic inelastic analysis of 3-D tunnels", *Soil Dyn. Earthq. Eng.*, **30**(9), 851-861. https://doi.org/10.1016/j.soildyn.2010.03.010.

Huang, S., Chen, W.Z., Wu, G.J., Guo, X.H. and Qiao, C.J. (2010), "Study of method of earthquake input in aseismic analysis for underground engineering", *Chin. J. Rock Mech. Eng.*, **29**(6), 1254-1262. (in Chinese)

Koizumi, A. (2009), *Seismic Research and Example of Shield Tunnelling*, China Architecture and Building Press, Beijing, China.

Koizumi, A. (2012), *The Segment Design of Shield Tunnelling*, China Architecture and Building Press, Beijing, China.

Kontoe, S., Zdravkovic, L., Potts, D.M. and Menkiti, C.O. (2008), "Case study on seismic tunnel response", *Can. Geotech. J.*, **45**(12), 1743-1764. https://doi.org/10.1139/T08-087.

Lai, J.X., He, S.Y., Qiu, J.L., Chen, J.X., Wang, L.X., Wang, K. and Wang, J.B. (2017), "Characteristics of seismic disasters and aseismic measures of tunnels in Wenchuan earthquake", *Environ. Earth. Sci.*, **94**(76), 1-19. https://doi.org/10.1007/s12665-017-6405-3.

Li, P. and Song, E.X. (2015), "Three-dimensional numerical analysis for the longitudinal seismic response of tunnels under an asynchronous wave input", *Comput. Geotech.*, **63**, 229-243. https://doi.org/10.1016/j.compgeo.2014.10.003.

Li, T.B. (2012), "Damage to mountain tunnels related to the Wenchuan earthquake and some suggestions for aseismic tunnel construction", *Bull. Eng. Geol. Environ.*, **71**(2), 297-308. https://doi.org/10.1007/s10064-011-0367-6.

Luco, J.E. and Barros, F.C.P. (1994), "Seismic response of a cylindrical shell embedded in a layered viscoelastic half-space. I: formulation", *Earthq. Eng. Struct. Dyn.*, **23**, 553-567. https://doi.org/10.1002/eqe.4290230507.

Pakbaz, M.C. and Yareevand, A. (2005), "2-D analysis of circular tunnel against earthquake loading", *Tunn. Undergr. Sp. Tech.*, **20**(5), 411-417. https://doi.org/10.1016/j.tust.2005.01.006.

Shalabi, F.I., Cording, E.J. and Paul, S.L. (2012), "Concrete segment tunnel lining sealant performance under earthquake loading", *Tunn. Undergr. Sp. Tech.*, **31**(5), 51-60. https://doi.org/10.1016/j.tust.2012.04.006.

Shalabi, F.I., Cording, E.J. and Paul, S.L. (2016), "Sealant behavior of gasketed segmental tunnel lining-Conceptual model", *Geomech. Tunnel.*, **9**(4), 345-355. https://doi.org/10.1002/geot.201500030.

Shen, Y.S., Gao, B., Yang, X.M. and Tao, S.J. (2016), "Seismic damage mechanism and dynamic deformation characteristic analysis of mountain tunnel after Wenchuan earthquake", *Eng. Geol.*, **180**, 85-98. https://doi.org/10.1016/j.enggeo.2014.07.017.

Stamos, A.A. and Beskos, D.E. (1996), "3-D seismic response analysis of long lined tunnels in half-space", *Soil Dyn. Earthq. Eng.*, **15**, 111-118. ttps://doi.org/10.1016/0267-7261(95)00025-9.

Tao, L.J., Hou, S., Zhao, X., Qiu, W.G., Li, T.B., Liu, C.X. and Wang, K. (2015), "3-D shell analysis of structure in portal section of mountain tunnel under seismic SH wave action", *Tunn. Undergr. Sp. Tech.*, **46**, 116-124. https://doi.org/10.1016/j.tust.2014.11.001.

Wang, W.L., Wang, T.T., Su, J.J., Lin, C.H., Seng, C.R. and Huang, T.H. (2001), "Assessment of damage in mountain tunnels due to the Taiwan Chi-Chi Earthquake", *Tunn. Undergr. Sp. Tech.*, **16**(3), 133-150. https://doi.org/10.1016/S0886-7798(01)00047-5.

Wang, Z. (2015), "Numerical study on waterproof failure mechanism of elastic sealing gasket of underwater shield-bored tunnel", *Tunn. Constr.*, **35**(11), 1164-1168. (in Chinese)

Yan, Q.X., Deng, Z.X., Zhang, Y.Y. and Yang, W.B. (2017), "Failure characteristics of joint bolts in shield tunnels subjected to impact loads from a derailed train", *Shock Vib.*, **9**, 1-17. https://doi.org/10.1155/2017/2829783.

Yan, Q.X., Li, B., Geng, P., Chen, C., He, C. and Yang, W.B. (2016), "Dynamic response of a double-lined shield tunnel to train impact loads", *Tunn. Undergr. Sp. Tech.*, **53**, 33-45. https://doi.org/10.1016/j.tust.2015.12.004.

Yan, Q.X., Song, L.Y., Chen, C., Chen, W.Y., Ma, S.Q. and Yang, W.B. (2018a), "Dynamic response of segment lining of overlapped shield tunnels under train-induced vibration loads", *Arab. J. Sci. Eng.*, **43**(10), 5439-5455. https://doi.org/10.1007/s13369-018-3147-9.

Yan, Q.X., Xu, Y.J., Zhang, W.L., Geng, P. and Yang, W.B. (2018b), "Numerical analysis of the cracking and failure behaviors of segmental lining structure of an underwater shield tunnel subjected to a derailed high-speed train impact", *Tunn. Undergr. Sp. Tech.*, **72**, 41-54. https://doi.org/10.1016/j.tust.2017.11.002.

Yang, Z.H., Lan, H.X., Zhang, Y.S., Gao, X. and Li, L.P. (2013), "Nonlinear dynamic failure process of tunnel-fault system in response to strong seismic event", *J. Asian Earth Sci.*, **64**, 125-135. https://doi.org/10.1016/j.jseaes.2012.12.006.

Yu, H.T., Chen, J.T., Bobet, A. and Yuan, Y. (2016), "Damage observation and assessment of the Longxi tunnel during the Wenchuan earthquake", *Tunn. Undergr. Sp. Tech.*, **54**, 102-116. https://doi.org/10.1016/j.tust.2016.02.008.

Yu, H.T., Yuan, Y. and Bobet A. (2017), "Seismic analysis of long tunnels: A review of simplified and unified methods", *Undergr. Sp.*, **2**(2), 73-87. https://doi.org/10.1016/j.undsp.2017.05.003.

Yu, H.T., Yuan, Y. and Bobet, A. (2013a), "Multiscale method for long tunnels subjected to seismic loading", *Int. J. Numer. Anal. Met.*, **37**(4), 374-398. https://doi.org/10.1002/nag.1102.

Yu, H.T., Yuan, Y., Qiao, Z.Z., Gu, Y., Yang, Z.H. and Li, X.D. (2013b), "Seismic analysis of a long tunnel based on multi-scale method", *Eng. Struct.*, **49**(2), 572-587. https://doi.org/10.1016/j.engstruct.2012.12.021.

Zhang, X.P., Jiang, Y.J. and Sugimoto, S. (2018), "Seismic damage assessment of mountain tunnel: A case study on the Tawarayama tunnel due to the 2016 Kumamoto Earthquake", *Tunn. Undergr. Sp. Tech.*, **71**, 138-148. https://doi.org/10.1016/j.tust.2017.07.019.

Zhao, W.S., Chen, W.Z., Huang, S. and Yang, F.D. (2010), "Research on method of seismic motion input in aseismic analysis for underground structure", *Chin. Civil Eng. J.*, **43**(s1), 554-559. (in Chinese)

KT